# Electronic structures and optical properties of low- and high-pressure phases of crystalline $B_2O_3$

Dong Li and W. Y. Ching
*Department of Physics, University of Missouri–Kansas City, Kansas City, Missouri 64110*
(Received 10 June 1996)

The high- and low-pressure phases of crystalline boron oxide $B_2O_3$ are investigated by first-principle calculations using a local-density approximation (LDA). Both phases are insulators with wide LDA band gaps of 6.20 eV for $B_2O_3$-I (low pressure) and 8.85-eV for $B_2O_3$-II (high pressure). The total density of states are calculated and resolved into atomic and orbital components. The bond strength and charge transfers in these two crystals are investigated by calculating the overlap populations and Mulliken effective charges. $B_2O_3$-II is found to be more ionic than $B_2O_3$-I. It is also concluded that the $sp^2$ planar bonding in $B_2O_3$-I is stronger than the $sp^3$ tetrahedral bonding in $B_2O_3$-II. The optical conductivities, the dielectric functions, and the energy-loss functions are also calculated using the wave functions at a large number of **k** points in the Brillouin zone. The calculated static dielectric constants for $B_2O_3$-I and $B_2O_3$-II are 2.32 and 2.35, respectively. The gross features of the optical spectra for the two crystals are quite similar with one marked difference. The $B_2O_3$-II crystal shows substantial optical anisotropy while $B_2O_3$-I is optically more isotropic. [S0163-1829(96)03143-8]

## I. INTRODUCTION

Boron oxides are important in ceramic and the glass industries mainly as components of special purpose glasses. The properties of vitreous boron oxide ($v$-$B_2O_3$), binary, or ternary borate glasses have been investigated mainly by optical spectroscopy.[1] It is well known that the transport properties of some borate glasses are affected by the nature of the ion carriers in the ''doping salt.'' [1] For example, the ionic conductivity of pure $v$-$B_2O_3$ glass is very small due to the lack of mobile charge carriers. However, the ionic conductivity can be increased drastically by the addition of a modifier alkali oxide. Borate glasses generally have rather complex structures. This complexity is caused mainly by a change in the coordination number of B atoms to the O ions which results in the formation of $[B\text{-}O_4]^-$ tetrahedra from the initial B-$O_3$ triangular groups.[2] These two kinds of polyhedra link together and form various connected ring structures. It is therefore important to understand the fundamental bonding structures in the boron compounds.

In contrast to the vast interest in borate glasses, there exist very few investigations on crystalline $B_2O_3$. There are two known crystalline forms obtained at low and high pressures.[3,4] Kracek, Morey, and Merwin concluded that spontaneous crystallization of $B_2O_3$ is not a simple process, since $B_2O_3$ does not crystallize readily from the highly dehydrated viscous melts.[5] MacKenzie and Claussen obtained a phase diagram consisting of two crystalline phases of $B_2O_3$ in the pressure range up to 80 kbar.[6] The low-pressure phase of $B_2O_3$ ($B_2O_3$-I) with a hexagonal unit cell [shown in Fig. 1(a)] was obtained at a pressure between 10 and 15 kbar and a high temperature up to 800 °C by Gurr, Montgomery, Knutson, and Gorres.[3] The structure consists of infinitely linked B-$O_3$ triangular units. The high-pressure phase of $B_2O_3$ ($B_2O_3$-II) was obtained at a pressure of 65 kbar and a temperature of 1100 °C by Prewitt and Shannon.[4] Figure 1(b) shows the crystal structure of $B_2O_3$-II which has an orthorhombic unit cell. The $B_2O_3$-II crystal consists of interconnected B-$O_4$ tetrahedra units with six- and eight-membered rings. The crystal parameters, the interatomic bond lengths, and bond angles for the two crystalline phases of $B_2O_3$ are summarized in Table I. In $B_2O_3$-I, the three B-O bond lengths within the B-$O_3$ planar are not the same. We separate B atoms into $B_1$ and $B_2$ types which give two slightly different B-$O_3$ units. The three O atoms bond to $B_1$ ($B_2$) are labeled as $O_1$, $O_2$, and $O_3$ ($O_{1'}$, $O_{2'}$, and $O_{3'}$). The B atom is at the center of three-nearest O with an average O-B-O angle of 119.97° and an average bridging angle for B-O-B of 130.71°. This O bridging angle is smaller than the O bridging angles in silicates. In $B_2O_3$-II, each B atom bonds to four O to form a distorted tetrahedron with one short bond of 1.373 Å and three longer bonds of 1.507, 1.506, and 1.512 Å.[4] The average B-O distance in $B_2O_3$-II is larger than that of $B_2O_3$-I in spite of the fact that $B_2O_3$-II has a much higher density. The O atoms in $B_2O_3$-II are divided into four types: $O_1$ bridges to two B atoms with the two shortest bonds. $O_2$, $O_{2'}$, and $O_{2''}$ each bond to three B atoms. Hence, there are 33.33% of bridging $O_1$ atoms and 66.67% of threefold bonded O atoms which bond to three B atoms in $B_2O_3$-II.

Recently, Takada *et al.* had applied the *ab initio* pseudopotential method to investigate the static structures of $B_2O_3$-I and $B_2O_3$-II crystals. Their calculation confirmed the structural transformation from the B-$O_3$ triangular unit into the B-$O_4$ tetrahedral unit after compression.[7] Unfortunately, their calculation does not provide information on the electronic structure of these two crystals. Grumbach, Sankey, and McMillan, using a plane-waves pseudopotential method in the local-density approximation (LDA), had elucidated the structure and electronic properties of $B_2O$ as an isoelectronic analog of carbon.[8] It was concluded that $B_2O$ has a body-centered tetragonal structure.

In this paper, we report the first-principles calculation of the electronic structure and optical properties of the two crystalline phases of $B_2O_3$. Earlier, we had studied the electronic structure and optical properties of rhombohedral $B_{12}O_2$ crystal.[9] In that case, the icosahedral $B_{12}$ units bond to two interstitial oxygen atoms. Thus the bonding configurations in $B_{12}O_2$, $B_2O_3$-I, and $B_2O_3$-II are quite different and it

 

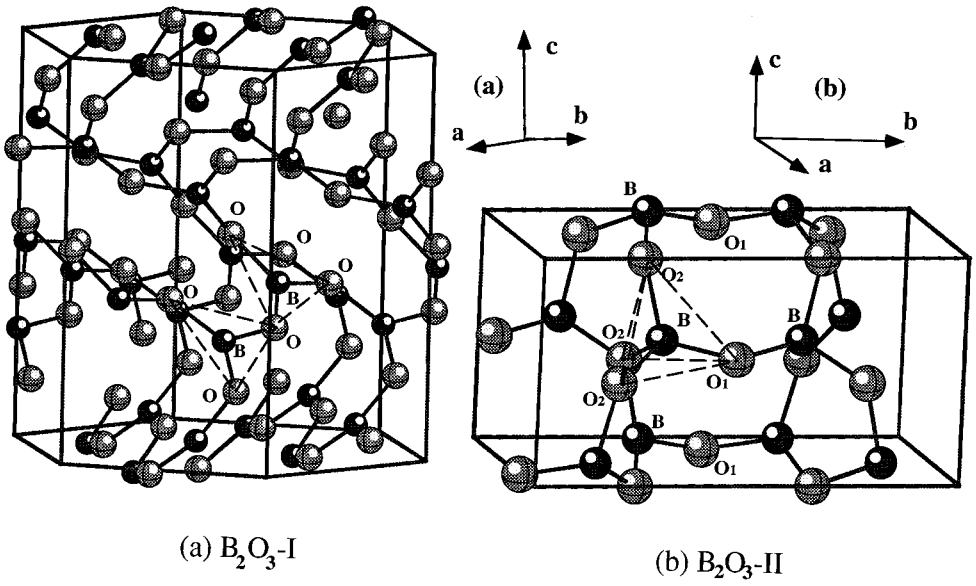


FIG. 1. Crystal structure of (a) $B_2O_3$-I, (b) $B_2O_3$-II. Two triangular units in (a) and one tetrahedral unit in (b) are outlined by dashed lines.

is of interest to compare and contrast their electronic properties.

## II. COMPUTATIONAL METHOD

We have used the first-principles orthogonalized linear combination of atomic orbital method in the LDA approximation to investigate the electronic and optical properties of $B_2O_3$-I and $B_2O_3$-II crystals. This LDA-based method for electronic structure calculation was well described[10] and has been successfully applied to study many complex ceramic crystals such as silicates,[11,12] nitrides,[12] titanates,[13,14] aluminates,[15–17] borates,[18] and $ZrO_2$,[19] etc. We briefly outline the major steps of our calculation. The Bloch functions were constructed from the atomic orbitals which were generated by separate self-consistant atomic calculations. Each atomic orbital consists of a linear combination of 16 Gaussian-type orbitals. Full basis sets consisting of $1s$, $2s$, $2p$, $3s$, and $3p$ orbitals of both B and O were used. A minimal basis set which consists of only the $2s$ and $2p$ orbitals of B and O is quite sufficient for the electronic structure study of the occupied states. To improve the accuracy, especially the higher conduction bands which are important for optical properties, extra orbitals of $3s$ and $3p$ were included in the basis set to increase the variational freedom. The potential and charge-density functions were fitted to a sum of atom-centered Gaussians. Fitting errors of less than a 0.001 electron per valence electron in the present calculations are achieved. For self-consistent iterations, six special-**k** points in the irreducible portion of the Brillouin-zone (BZ) were used. For the final density of states (DOS's) and optical calculations, energy eigenvalues and eigenfunctions at 95 and 125 regularly spaced **k** points in the same irreducible part of the BZ were obtained for $B_2O_3$-I and $B_2O_3$-II, respectively. The DOS's were obtained by using the linear analytical tetrahedron method and the partial DOS's (PDOS's) were projected using the Mulliken procedure.[20]

It is instructive to study the charge transfer and the bond strength in the $B_2O_3$ crystals by calculating the effective charges on each atom and the overlap populations (or bond order) between pairs of atoms. The bond order is a simple way to estimate the relative strengths of the bonding. Negative values indicate that antibonding may exist between the pairs. We have already used this approach to study the electronic structure and bonding in the boron-rich compounds $B_{12}As_2$, $B_{12}P_2$, $B_{13}C_2$, $B_{11}C$(CBC) (Ref. 21), and $B_{12}O_2$.[9] The effective charge $Q_\delta^*$ on atom $\delta$ and the overlap population $\rho_{\gamma,\delta}$ between atoms $\gamma$ and $\delta$ are defined as

$$Q_\delta^* = \sum_{n=\text{occ.}} \sum_i \sum_{j,\gamma} \sum_{\mathbf{k}} W(\mathbf{k}) (A_{i,\gamma}^n)^* A_{j,\delta}^n S_{i\gamma,j\delta}(\mathbf{k}), \quad (1)$$

$$\rho_{\gamma,\delta} = \sum_{n=\text{occ.}} \sum_i \sum_j \sum_{\mathbf{k}} W(\mathbf{k}) (A_{i,\gamma}^n)^* A_{j,\delta}^n S_{i\gamma,j\delta}(\mathbf{k}), \quad (2)$$

where $W(\mathbf{k})$ is the **k** point weighting factor and the summation over **k** is for the entire BZ. $A_{i,\gamma}$ are the eigenfunction coefficients and $S_{i\gamma,j\delta}(\mathbf{k})$ are the overlap integrals at **k**. $i$ and $j$ are the orbital specifications for the state. Since the calculations for $Q_\delta^*$ and $\rho_{\gamma,\delta}$ are based on Mulliken analysis,[20] which is more accurate when the basis functions are relatively localized, we used the minimal basis set rather than a full basis for the calculation of $Q_\delta^*$ and $\rho_{\gamma,\delta}$.

From the energy eigenvalues and wave functions, the real part of the frequency-dependent interband optical conductivity $\sigma(\omega)$ can be obtained from Eq. (3),

$$\sigma(\hbar\omega) = \frac{e^2}{(2\pi)^2 \mu \hbar \omega} \int d\mathbf{k} \sum_{n,m} |\langle \psi_m(\mathbf{k},\mathbf{r}) | \mathbf{p} | \psi_n(\mathbf{k},\mathbf{r}) \rangle|^2 \times f_n(\mathbf{k})[(1 - f_m(\mathbf{k})]\delta[E_m(\mathbf{k}) - E_n(\mathbf{k}) - \hbar\omega], \quad (3)$$

where $\hbar\omega$ is the photon energy, and $f_n$ is the Fermi function for the state $n$. The optical matrix elements were evaluated at each **k** point and the integration over the BZ was performed using the linear analytic tetrahedron method. Since a fairly large number of **k** points were used, the resolution of the calculated optical spectra is more than sufficient. The imaginary part of the dielectric function $\varepsilon_2(\omega)$ was obtained from

TABLE I. Crystal data of $B_2O_3$-I and $B_2O_3$-II.

| Crystals | $B_2O_3$-I (a) | $B_2O_3$-II (b) |
|---|---|---|
| Lattice constant | $a=4.336$ (Å) | $a=4.613$ (Å) |
| | $c=8.340$ (Å) | $b=7.803$ (Å) |
| | | $c=4.129$ (Å) |
| Density ($g/cm^3$) | 2.56 | 3.11 |
| Cell volume ($Å^3$) | 135.79 | 148.62 |
| Space group | $P3_1$ ($Z=3$) | Ccm2 ($Z=4$) |
| Bond distances (Å) | $B_1$-$O_1$: 1.404 | B-$O_1$: 1.373 |
| (nearest) | -$O_2$: 1.366 | -$O_2$: 1.507 |
| | -$O_3$: 1.337 | -$O_{2'}$: 1.506 |
| | (Ave. $B_1$-O: 1.369) | -$O_{2''}$: 1.512 |
| | B2-$O_{1'}$: 1.336 | (Ave. B-O: 1.475) |
| | -$O_{2'}$: 1.401 | $O_1$-$O_2$: 2.364 |
| | -$O_{3'}$: 1.384 | $O_1$-$O_{2'}$: 2.440 |
| | (Ave. $B_2$-O: 1.374) | $O_1$-$O_{2''}$: 2.409 |
| | $O_1$-$O_2$: 2.387 | $O_2$-$O_{2'}$: 2.428 |
| | $O_1$-$O_3$: 2.309 | $O_2$-$O_{2''}$: 2.394 |
| | $O_2$-$O_3$: 2.409 | $O_{2'}$-$O_{2''}$: 2.388 |
| | $O_{1'}$-$O_{2'}$: 2.388 | (Ave. O-O: 2.404) |
| | $O_{1'}$-$O_{3'}$: 2.409 | B-B: 2.569 |
| | $O_{2'}$-$O_{3'}$: 2.333 | : 2.664 |
| | (Ave. O-O: 2.373) | : 2.664 |
| | $B_1$-$B_2$: 2.489 | : 2.592 |
| | : 2.498 | (Ave. B-B: 2.608) |
| Bond angles | $O_1$-$B_1$-$O_2$: 119.03° | $O_1$-B-$O_2$: 110.19° |
| | $O_1$-$B_1$-$O_3$: 114.73° | $O_1$-B-$O_{2'}$: 115.79° |
| | $O_2$-$B_1$-$O_3$: 126.10° | $O_1$-B-$O_{2''}$: 113.18° |
| | $O_{1'}$-$B_2$-$O_{2'}$: 121.47° | (Ave. $O_1$-B-$O_2$: 113.53°) |
| | $O_{1'}$-$B_2$-$O_{3'}$: 124.66° | $O_2$-B-$O_{2'}$: 107.34° |
| | $O_{2'}$-$B_2$-$O_{3'}$: 113.84° | $O_2$-B-$O_{2''}$: 104.94° |
| | [Ave. O-$B_1$($B_2$)-O: 119.97°] | $O_{2'}$-B-$O_{2''}$: 104.64° |
| | $B_1$-$O_1$($O_{1'}$)-$B_2$: 130.49° | (Ave. $O_2$-B-$O_2$: 105.64°) |
| | $B_1$-$O_2$($O_{2'}$)-$B_2$: 128.29° | B-$O_1$-B: 138.59° |
| | $B_1$-$O_3$($O_{3'}$)-$B_2$: 133.34° | B-$O_2$-B: 123.78° |
| | (Ave. $B_1$-O-$B_2$: 130.71°) | B-$O_{2'}$-B: 123.79° |
| | | B-$O_{2''}$-B: 118.69° |
| | | (Ave. B-$O_2$-B: 122.02°) |
| Ring structure | 20 | 6,8 |

[a]Reference 3.
[b]Reference 4.

$\varepsilon_2(\omega)=(4\pi/\omega)\sigma(\omega)$ and the real part $\varepsilon_1(\omega)$ was extracted from $\varepsilon_2(\omega)$ using the Kramers-Kronig relation. The electronic-energy loss function was then obtained from both the real and imaginary parts of the dielectric function.

## III. CALCULATED RESULTS OF $B_2O_3$-I AND $B_2O_3$-II

### A. Electronic structures

The calculated band structures along the high-symmetry axes of the BZ for $B_2O_3$-I and $B_2O_3$-II are shown in Fig. 2. Both crystals are wide gap insulators with calculated LDA gaps of about 6.20 and 8.85 eV, respectively. For $B_2O_3$-I ($B_2O_3$-II), the top of the valence band (VB) is at a point along $\Gamma K$ ($\Gamma R$) and the bottom of the conduction band is at $A$ ($\Gamma$). Both are very flat with little dispersion indicating

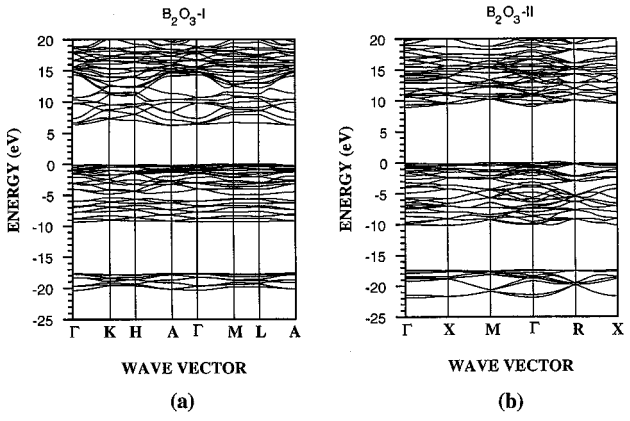


FIG. 2. Calculated band structures of (a) $B_2O_3$-I, (b) $B_2O_3$-II.

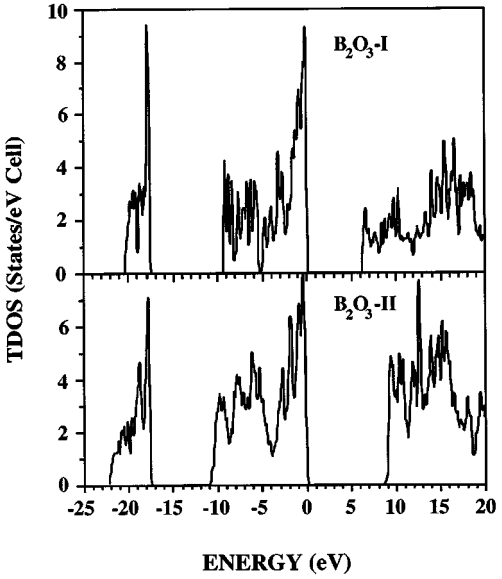


FIG. 3. Calculated total DOS's of (a) $B_2O_3$-I, (b) $B_2O_3$-II.

large effective masses for the carriers. Our recent calculations on $B_{12}O_2$ (Ref. 9) show it to be a semiconductor with a gap of 2.40 eV. Obviously, the icosahedral $B_{12}$ unit in $B_{12}O_2$ is a unique structure with a completely different bonding pattern and a very different band structure.

The total DOS's (TDOS's) of $B_2O_3$-I and $B_2O_3$-II are compared in Fig. 3. Both crystals have very sharp VB and conduction-band edges. For $B_2O_3$-I, there are three segments within the VB (start from the top of VB) with the widths of 5.16, 4.64, and 3.25 eV separately. These segments account for 36, 18, and 18 electrons, respectively, for a total of 72 valence electrons. The gap between the first and second segments, however, is only 0.3 eV. This gap is the signature of O atom in a bridging position whose $2p$ orbitals can be divided into bonding and nonbonding parts, as is common in many oxides.[11,12] For $B_2O_3$-II, there are only two segments within the same VB region. The bonding and nonbonding parts of the O-$2p$ orbitals have coalesced together. This is because in $B_2O_3$-II, only one-third of the O atoms are the bridging O with the rest of the O atoms bond to three B atoms. There are 72 valence electrons occupying the first segment with a total width of 10.91 eV, which is about 1 eV larger than the combined widths of the first two segments in $B_2O_3$-I. The second segment which accounts for 24 electrons is 1.5 eV wider than the third segment in $B_2O_3$-I. We have listed the widths of each band segment and total widths of the VB for both crystals in Table II.

The orbital-resolved PDOS's for $B_2O_3$-I are presented in Fig. 4. The PDOS's in the figure actually include the $3s$ and $3p$ components. However, the $2s$ and $2p$ orbitals dominate in the VB region and for clarity in the discussion, we simply refer to as $2s$ and $2p$ orbitals of B and O. It is clear that B-$2s$ orbitals distribute over the second and third segments while B-$2p$ orbitals contribute to all three segments. Also, B-$2s$ and B-$2p$ hybrid with each other within the second and third segments. The lowest segment is dominated by the O-$2s$ electrons which interact with both B-$2s$ and B-$2p$ orbitals. The O-$2p$ orbitals dominate the first two segments. Although there are two distinct B-$O_3$ triangles in the $B_2O_3$-I structure,[3] we find that their PDOS's are almost identical since the bond

TABLE II. Calculated band gaps, bandwidths, static dielectric constants $\varepsilon_0$, and the bulk-plasmon frequency $\omega_p$ of $B_2O_3$-I and $B_2O_3$-II.

| Crystal | $B_2O_3$-I | $B_2O_3$-II |
|---|---|---|
| Band gap Eg (eV) | 6.20 | 8.85 |
| Width of valence band | $W_1$: 5.16 | $W_1$: 10.91 |
| (eV) | $W_2$: 4.64 | $W_2$: 4.81 |
| | $W_3$: 3.25 | |
| Width of total VB (eV) | 20.60 | 22.21 |
| | 2.32 | 2.35 |
| $\varepsilon_0$ | 2.34 ($x$-$y$) | 2.30 ($x$) |
| | 2.30 ($z$) | 2.43 ($y$) |
| | | 2.31 ($z$) |
| $\omega_p$ (eV) | 23.5; 26.5 | 25.0 |

lengths and bond angles are very similar as shown in Table I. Figure 5 shows the PDOS's of $B_1$-$2s$, $B_1$-$2p$, $O_1$-$2s$, $O_1$-$2p$, $O_2$-$2s$, and $O_2$-$2p$ for the $B_2O_3$-II crystal which are quite different from that of $B_2O_3$-I. Both $B_1$-$2s$ and $B_1$-$2p$ have distributions only at the lower part of the top segment. The shapes of the PDOS's are also quite different from $B_2O_3$-I reflecting the different bonding environments. The distributions for the PDOS's of $B$ are much more broad. In particular, there is little contribution within the 0 to $-3.5$ eV region while in $B_2O_3$-I, B-$2s$ has a substantial contribution in the same region. At the CB edge, B-$s$ orbitals have a substantial contribution which is not the case in $B_2O_3$-I. For the O atom, there are substantial differences in the PDOS's of $O_1$ which is a bridging O with a very short bond length and $O_2$ which bond to three B atoms with a longer bond length. It is also noted that the PDOS's of $O_1$ is similar to the PDOS's of O in $B_2O_3$-I since both are bridging O. The PDOS's of $O_1$-$2p$ again shown the signature of bonding and nonbonding parts

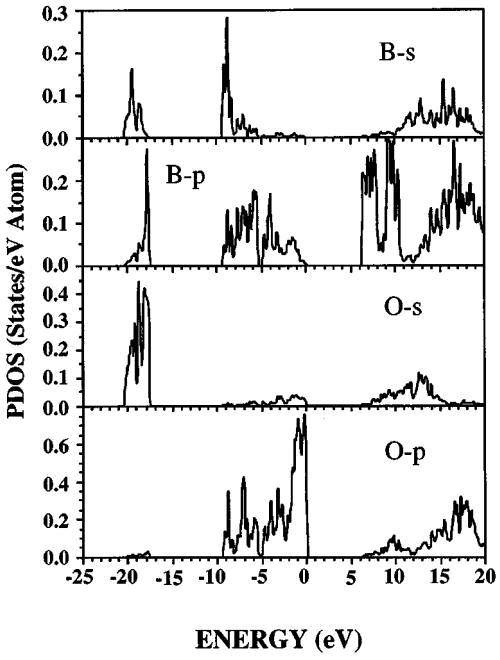


FIG. 4. Calculated partial DOS's of $B_2O_3$-I. $3s$ and $3p$ orbital components are included.

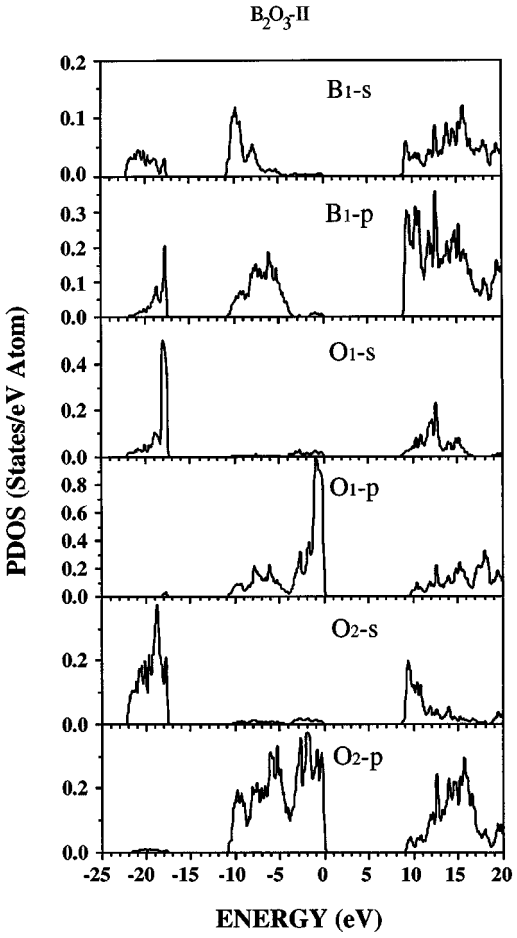


FIG. 5. Calculated partial DOS's of $B_2O_3$-I. $3s$ and $3p$ orbital components are included.

separated by a dip near $-4.0$ eV. Another interesting observation is that in the case of $B_{12}O_2$,[9] the O-$2s$ level is at $-23.5$ eV and does not mix with either B-$2s$ or B-$2p$ orbitals. For $B_2O_3$-I or $B_2O_3$-II, however, B-$2s$, B-$2p$, and O-$2s$ have contributions to the much broader third segment centered at $-20$ eV. These differences all underscore the different type of bonding in the three boron oxides. In $B_2O_3$-I, it is the B-$O_3$ bonding; in $B_2O_3$-II, it involves B-$O_4$ tetrahedral bonding and in $B_{12}O_2$, it is a partially covalent bonding of O to three icosahedral $B_{12}$ units.

The calculated Mulliken effective charges for $B_2O_3$-I and $B_2O_3$-II are listed in Table III. In $B_2O_3$-I, each B atom loses a 0.71 electron to the neighboring O. $O_1$, $O_2$, and $O_3$ each gain 0.45, 0.46, and 0.51 electrons respectively. The difference is attributed to the slight distortion of the B-$O_3$ triangular unit. In $B_2O_3$-II, each B atom lose almost one electron. The bridging atom $O_1$ with the shortest bond length gains a 0.66 electron, while $O_2$, $O_{2'}$, and $O_{2''}$ each gain a 0.58 electron, although the bond length for B-$O_2$, B-$O_{2'}$, and B-$O_{2''}$ are slightly different. On average, the effective charge calculation has shown $B_2O_3$-II to be more ionic than $B_2O_3$-I.

TABLE III. Calculated effective charge $Q_\delta^*$ for $B_2O_3$-I and $B_2O_3$-II.

| $B_2O_3$-I | $B_2O_3$-II |
|---|---|
| 2.29 ($B_1$) | 2.09 (B) |
| 2.29 ($B_2$) | 6.66 ($O_1$) |
| 6.45 ($O_1$ or $O_{1'}$) | 6.58 ($O_2$) |
| 6.46 ($O_2$ or $O_{2'}$) | 6.58 ($O_{2'}$) |
| 6.51 ($O_3$ or $O_{3'}$) | 6.58 ($O_{2''}$) |

TABLE IV. Calculated overlap populations $\rho_{\gamma,\delta}$ for $B_2O_3$-I and $B_2O_3$-II.

| $B_2O_3$-I | $B_2O_3$-II |
|---|---|
| 0.17 ($B_1$-$O_1$) | 0.20 (B-$O_1$) |
| 0.20 ($B_1$-$O_2$) | 0.14 (B-$O_2$) |
| 0.21 ($B_1$-$O_3$) | 0.14 (B-$O_{2'}$) |
| 0.21 ($B_2$-$O_{1'}$) | 0.13 (B-$O_{2''}$) |
| 0.17 ($B_2$-$O_{2'}$) | |
| 0.19 ($B_2$-$O_{3'}$) | |

The overlap populations between different B-O pairs in $B_2O_3$-I and $B_2O_3$-II are calculated according to Eq. (2). The results are listed in Table IV. In $B_2O_3$-I, $B_1$-$O_3$ and $B_2$-$O_{1'}$ have the largest bond order values of 0.21 and $B_1$-$O_1$ and $B_2$-$O_{2'}$ have the smallest value of 0.17. $B_1$-$O_2$ and $B_2$-$O_{3'}$ have intermediate values of 0.20 and 0.19. Apparently, the bond order for the triangular unit in $B_2O_3$-I scales inversely with interatomic separations. For $B_2O_3$-II, the largest bond order is 0.20 for $B_1$-$O_1$, while the smallest value is 0.13 for $B_1$-$O_{2''}$. Hence, on average, the bond strength in $B_2O_3$-II is weaker than that in $B_2O_3$-I. It is thus concluded that planar $sp^2$ bonding in $B_2O_3$-I is stronger than the $sp^3$ tetrahedral bonding in $B_2O_3$-II. The bond order for a B-O pair in the $B_{12}O_2$ crystal is 0.17.[9]

Figure 6 displays the calculated valence charge-density map for a plane that approximately contains a B-$O_3$ unit in $B_2O_3$-I. We can actually identify three B-$O_3$ units linked together, but two of them are slightly off the plane. It can be seen that the valence charge distribution of O is no longer spherical with the charge drawn in the direction towards the B atom. This is further evidence that the triangular B-$O_3$ bonding in $B_2O_3$-I has some covalent character which strengthens the bond. The charge density in the middle of the B-O bond is 0.11 $e$/(a.u.)$^3$. A similar valence charge-density contour for $B_2O_3$-II is shown in Fig. 7. The plane passes

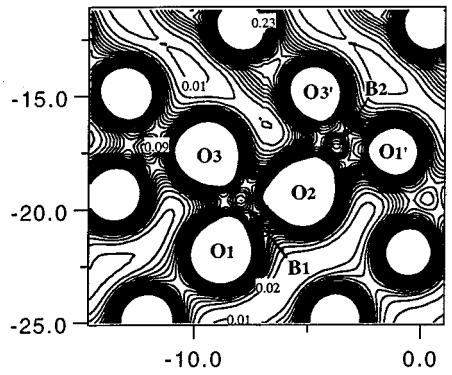


FIG. 6. Charge-density contours in a plane containing a B-$O_3$ unit in $B_2O_3$-I. The contour lines range from 0.01 to 0.25 $e$/(a.u.)$^3$ in intervals of 0.01.

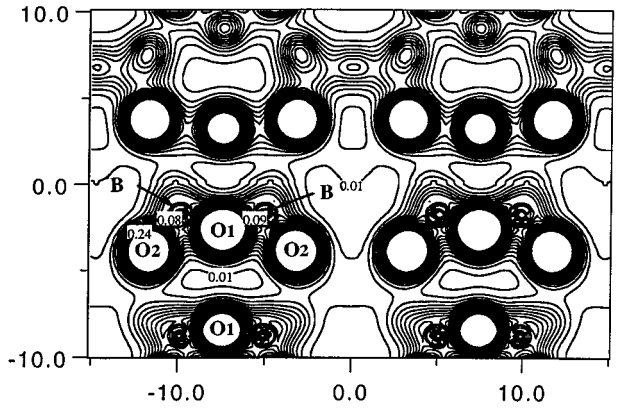


FIG. 7. Charge-density contours in a plane containing a B-O-B unit in $B_2O_3$-II. The units are the same as in Fig. 6.

three atoms forming the B-O-B bonding. The charge density in the middle of the B-$O_1$ (B-$O_2$) bonding is 0.09 (0.07) e/(a.u.)$^3$. The charge-density distributions in $B_2O_3$-II is quite different from that of $B_2O_3$-I in Fig. 6. In particular, the distribution on the O atom is more spherical in $B_2O_3$-II, reflecting a higher symmetric configuration of the B-$O_4$ tetrahedral unit.

### B. Optical properties

We have calculated the interband optical conductivity $\sigma(\omega)$ of $B_2O_3$-I and $B_2O_3$-II crystals for photon energies up to 40 eV according to Eq. (3). The $\sigma(\omega)$ for $B_2O_3$-I is shown in Fig. 8(a). The calculated absorption threshold is about 6.40 eV which is 0.20 eV larger than the minimal indirect gap. A sharp peak at 6.63 eV immediately after the sharp threshold is noted. Other major structures are located at 11.7, 17.3, and 32.4 eV with many additional smaller structures in between. The real and imaginary parts of the dielectric function obtained from $\sigma(\omega)$ are plotted in Fig. 8(b). The static dielectric constant $\varepsilon_0$ of 2.32 is obtained from the zero-frequency limit of $\varepsilon_1(\omega)$. Figure 8(c) shows the energy-loss function. Two major plasmon peaks around 23.5 and 26.5 eV can be identified.

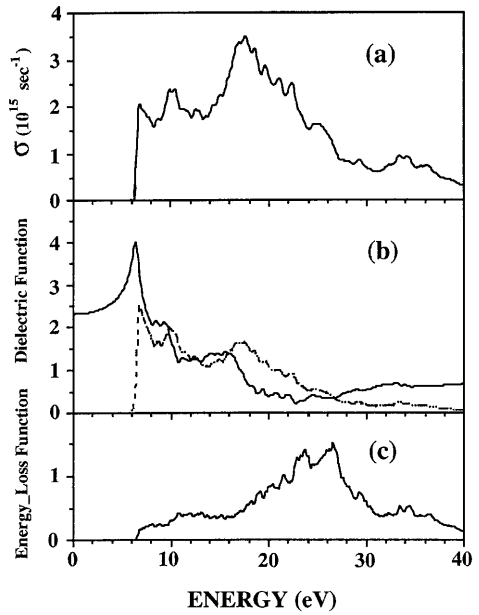


FIG. 8. Calculated optical properties of $B_2O_3$-I: (a) $\sigma(\omega)$, (b) $\varepsilon_1(\omega)$ (solid line) and $\varepsilon_2(\omega)$ (dashed line), and (c) the energy-loss function.

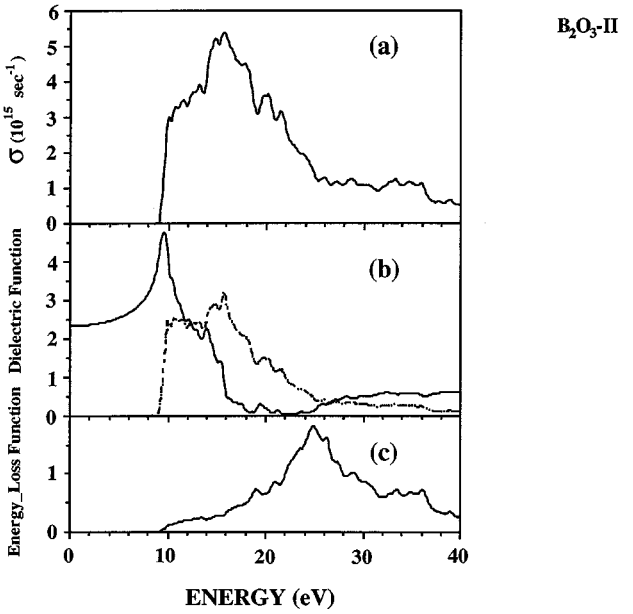


FIG. 9. Calculated optical properties of $B_2O_3$-II: (a) $\sigma(\omega)$, (b) $\varepsilon_1(\omega)$ (solid line) and $\varepsilon_2(\omega)$ (dashed line), and (c) the energy-loss function.

The calculated $\sigma(\omega)$ for $B_2O_3$-II is shown in Fig. 9(a). The absorption threshold is again very sharp starting at 9.03 eV, which is close to the band gap of 8.86 eV. This curve is somewhat different from $B_2O_3$-I with one major peak at 15.7 eV. The gross features of the two $\sigma(\omega)$ curves for the two crystals are quite similar. This peak is 1.6 eV lower than the major peak in $B_2O_3$-I. There are several additional structures on either side of the broad peak. The real and imaginary dielectric functions are plotted in Fig. 9(b), with a static dielectric constant $\varepsilon_0$ of 2.35. This value is very close to the $\varepsilon_0$ value of 2.32 for $B_2O_3$-I. This is quite surprising, considering the difference in the band gaps of the two crystals. Both of the calculated $\varepsilon_0$ are smaller than the value of 3.40 for the icosahedral $B_{12}O_2$ crystal.[9] The energy-loss function of $B_2O_3$-II in Fig. 9(c) shows a single bulk-plasmon peak at 25.0 eV, which is between the two plasmon peaks in $B_2O_3$-I. Comparing the calculated $\varepsilon_0$ and $\omega_p$ of $B_2O_3$-I and $B_2O_3$-II with the other B-rich compounds such as $\alpha$-$r$-$B_{12}$, $B_{12}As_2$, $B_{12}P_2$, $B_{13}C_2$, and $B_{11}C(CBC)$,[21,22] we notice that $\varepsilon_0$ and $\omega_p$ of $B_2O_3$-I, $B_2O_3$-II, and $B_{12}O_2$ are all relatively smaller. We attribute this to the more ionic bonding changes associated with the oxygen atoms. We found that the experimental values for the static dielectric constant of $B_2O_3$-I and $B_2O_3$-II were quoted as between 3.0 and 3.5.[23] Our calculated values of 2.32 and 2.35 are smaller than the quoted values. It is conceivable that the measurements were carried out at finite frequencies which have a larger value of $\varepsilon_1(\omega)$ than $\varepsilon_1(0)$. The calculated $\varepsilon_0$ and $\omega_p$ of $B_2O_3$-I and $B_2O_3$-II are listed in Table II.

To study the possible optical anisotropies in $B_2O_3$-I and $B_2O_3$-II crystals, we resolve the imaginary dielectric function of the hexagonal of $B_2O_3$-I in the $x$-$y$ plane and along the $z$

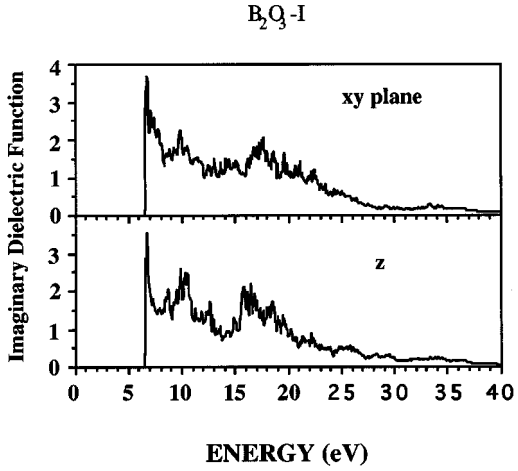


FIG. 10. Calculated components of $\varepsilon_2(\omega)$ in $B_2O_3$-I.

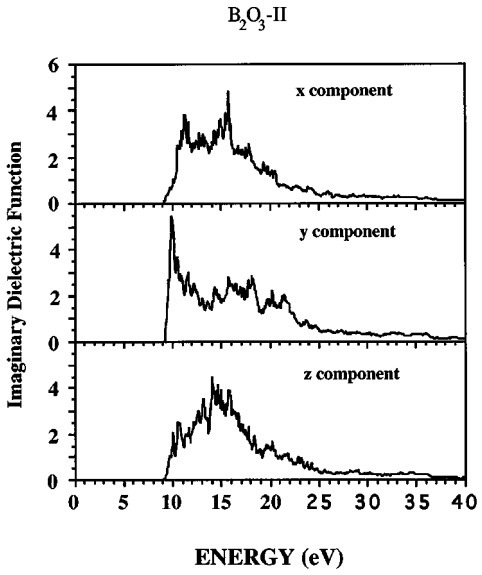


FIG. 11. Calculated components of $\varepsilon_2(\omega)$ in $B_2O_3$-II.

axis, and the orthorhombic $B_2O_3$-II in components parallel to the $x$, $y$, and $z$ axes. These are displayed in Fig. 10 and Fig. 11, respectively. No substantial anisotropy is found in $B_2O_3$-I. However, the $x$, $y$, and $z$ components of $\varepsilon_2(\omega)$ for $B_2O_3$-II show a considerable difference. In particular, the $y$ component of $\varepsilon_2(\omega)$ shows a much steeper edge at the threshold than the $x$ or $z$ component. The major peak positions in the spectra for the three compounds are also very different. We speculate that the difference in the optical anisotropy between $B_2O_3$-I and $B_2O_3$-II is mainly due to the difference in the local bonding units. In $B_2O_3$-I, O are all in bridging position connecting the B-$O_3$ triangular units, while in $B_2O_3$-II two-thirds of the O are bonded to three B atoms at the centers of the B-$O_4$ tetrahedral units.

## IV. CONCLUSIONS

We have studied the electronic structure and optical properties of the two crystalline forms of $B_2O_3$. The low-pressure phase $B_2O_3$-I and the high-pressure phase $B_2O_3$-II have rather different DOS's and PDOS's because of different local bonding configurations. Both are wide gap insulators with LDA gaps of 6.20 and 8.85 eV, respectively. Effective charge and bond order calculations show $B_2O_3$-I to be less ionic and show partial covalent character. Optical properties calculation shows similar optical conductivity curves with sharp edges at the threshold and similar static dielectric constants for both crystals. $B_2O_3$-I shows little optical anisotropy while $B_2O_3$-II shows considerable optical anisotropy possibly because of the more complicated local bonding structure. We anticipate the electronic structure and optical properties of pure $v$-$B_2O_3$ to be close to that of the $B_2O_3$-I.

## ACKNOWLEDGMENTS

This work was supported by U.S. Department of Energy under the Grant No. DE-FG02-84DR45170, and also in part by the UMKC Faculty Research Grant.

[1] M. Massot and M. Balkanski, in *Disorder in Condensed Matter Physics*, edited by J. A. Blackman and J. Tagüeña (Oxford, New York, 1991), p. 74.
[2] *Optical Constants of Inorganic Glasses*, edited by A. M. Efimov (CRC, New York, 1995), p. 88.
[3] G. E. Gurr, P. W. Montgomery, C. D. Knutson, and B. T. Gorres, Acta Crystallogr. Sec. B **26**, 906 (1970).
[4] C. T. Prewitt and R. D. Shannon, Acta Crystallogr. Sec. B **24**, 869 (1968).
[5] F. C. Kracek, G. W. Morey, and H. E. Merwin, Am. J. Sci. **35A**, 143 (1938).
[6] J. D. MacKenzie and W. F. Claussen, J. Am. Ceram. Soc. **44**, 79 (1961).
[7] A. Takada, C. R. A. Catlow, J. S. Lin, G. D. Price, M. H. Lee, V. Milman, and M. C. Payne, Phys. Rev. B **51**, 1447 (1995).
[8] M. P. Grumbach, O. F. Sankey, and P. F. McMillan, Phys. Rev. B **52**, 15 807 (1995).
[9] D. Li and W. Y. Ching, Phys. Rev. B **54**, 1451 (1996).
[10] W. Y. Ching, J. Am. Ceram. Soc. **73**, 3135 (1990).
[11] Y.-N. Xu and W. Y. Ching, Phys. Rev. B **44**, 11 048 (1991).
[12] Y.-N. Xu and W. Y. Ching, Phys. Rev. B **51**, 17 379 (1995).
[13] W. Y. Ching and Y.-N. Xu, Phys. Rev. B **44**, 5332 (1991).
[14] Shang-di Mo and W. Y. Ching, Phys. Rev. B **51**, 13 023 (1995).
[15] W. Y. Ching, Z.-Q. Gu, and Y.-N. Xu, Phys. Rev. B **50**, 1992 (1994).
[16] Y.-N. Xu and W. Y. Ching, Phys. Rev. B **43**, 4461 (1991).
[17] W. Y. Ching and Y.-N. Xu, J. Am. Ceram. Soc. **77**, 404 (1994).
[18] Y.-N. Xu, W. Y. Ching, and R. H. French, Phys. Rev. B **48**, 17 695 (1993).
[19] R. H. French, S. J. Glass, F. S. Oguchi, Y.-N. Xu, and W. Y. Ching, Phys. Rev. B **49**, 5133 (1994).
[20] R. S. Mulliken, J. Am. Chem. Soc. **77**, 887 (1954).
[21] D. Li and W. Y. Ching, Phys. Rev. B **52**, 17 073 (1995).
[22] D. Li, Y.-N. Xu, and W. Y. Ching, Phys. Rev. B **45**, 5895 (1992).
[23] *The Oxide Handbook*, edited by G. V. Samsonov (Plenum, New York, 1982).